Applied Physics Letters ARTICLE scitation.org/journal/apl

Electroresistance in metal/ferroelectric/semiconductor tunnel junctions based on a $Hf_{0.5}Zr_{0.5}O_2$ barrier

Cite as: Appl. Phys. Lett. **118**, 252901 (2021); doi: 10.1063/5.0053959
Submitted: 13 April 2021 · Accepted: 4 June 2021 ·
Published Online: 21 June 2021

View Online Export Citation CrossMark

Peijie Jiao, Zhongnan Xi, Xiaoyu Zhang, Yajie Han, Yang Wu, and Di Wu[a)]

AFFILIATIONS

National Laboratory of Solid State Microstructures, Department of Materials Science and Engineering, and Jiangsu Key Laboratory of Artificial Functional Materials, Nanjing University, Nanjing 210093, China

[a)]Author to whom correspondence should be addressed: diwu@nju.edu.cn

ABSTRACT

Ferroelectric $Hf_{0.5}Zr_{0.5}O_2$ films, 5.8 nm in thickness, were deposited on Nb:$SrTiO_3$ semiconductor substrates to form a Pt/$Hf_{0.5}Zr_{0.5}O_2$/Nb:$SrTiO_3$ metal/ferroelectric/semiconductor ferroelectric tunnel junction (FTJ). A high tunneling electroresistance ratio of 800 was achieved at room-temperature. It is observed that in the low resistance state, the transport characteristic obeys direct tunneling, while in the high resistance state, it is dominated by thermal emission. It implies that the Schottky barrier on the surface of the semiconductive electrode is modulated by the polarization in the ferroelectric $Hf_{0.5}Zr_{0.5}O_2$ barrier, generating the high electroresistance ratio. The FTJ also exhibits excellent retention for more than 10 000 s and good switching endurance for more than 1500 cycles. The results suggest the potential of this HfO_2-based FTJ for next generation nonvolatile memories.

HfO_2-based ferroelectric films have drawn great interest since their discovery in Si-doped HfO_2.[1] In contrast to conventional perovskite ferroelectrics, HfO_2-based ferroelectric films show advantages such as stable ferroelectricity in ultrathin films[2] and compatibility with complementary metal-oxide-semiconductor processes.[3] Following the seminal work on Si-doped HfO_2, various dopants, such as Zr,[4] Al,[5] Y,[6] La,[7] Gd,[8] and Sr,[9] have been reported to induce ferroelectricity in HfO_2-based films. Among them, Zr-doped HfO_2 has been intensively studied for its robust ferroelectricity as the formation of a metastable orthorhombic phase or a rhombohedral phase.[4,10] HfO_2-based ferroelectrics have also been further proposed for various applications such as nonvolatile memories,[11] negative capacitance field effect transistors,[12] high-electron-mobility transistors,[13] and energy storage capacitors.[14] For nonvolatile memories, ferroelectric tunnel junctions (FTJs), having advantages of both ferroelectric memories and resistive memories, are considered a promising candidate for next generation nonvolatile memories.[15,16]

An FTJ consists of a thin ferroelectric barrier layer sandwiched between two conductive electrodes, as first proposed by Esaki in 1971.[17] Due to the incomplete screening of the polarization, the barrier height of a tunnel junction is modulated by the depolarizing field, which is opposite to the polarization direction in the ferroelectric barrier.[18] The change in the barrier height significantly alters the tunneling probability and the junction resistance, which is commonly evaluated by the tunneling electroresistance (TER) ratio. It is worth noting that the two electrodes of a FTJ should have different screening lengths and the TER ratio increases with the asymmetry in the two ferroelectric/electrode interfaces. In this respect, metal/ferroelectric/semiconductor FTJs, replacing one of the metallic electrodes with a semiconductor, have been proposed.[19,20] In metal/ferroelectric/semiconductor FTJs, there is an extra Schottky barrier at the ferroelectric/semiconductor interface when the semiconductor surface is depleted by the polarization charge in the barrier. Therefore, both the width and the height of the barrier can be controlled in response to the reversal of the ferroelectric polarization, thereby significantly improving the TER effect.

Since ferroelectric properties of HfO_2-based films maintain in nanometer thickness, it is natural to use them as barriers in FTJs.[21,22] However, only a few HfO_2-based FTJs have been reported using a semiconductor as electrodes. Compared with FTJs using perovskite ferroelectric barriers that exhibit a huge TER ratio of about 10^7 (Refs. 20 and 23) and realize a sub-nanosecond resistance switchings[24] at room temperature, HfO_2-based metal/ferroelectric/semiconductor FTJs have shown a relatively low TER ratio around 10 in previous

reports.[25,26] In this work, we deposited $Hf_{0.5}Zr_{0.5}O_2$ (HZO) films directly on Nb-doped $SrTiO_3$ (Nb:STO) semiconductor substrates to fabricate Pt/HZO/Nb:STO FTJs. Ferroelectric properties of the HZO films and memory effects of the FTJs are characterized and discussed.

The structure of the Pt/HZO/Nb:STO FTJs is shown schematically in Fig. 1(a). The ultrathin HZO films were deposited on (001)-oriented Nb:STO, with 0.1% Nb in concentration, single crystalline substrates by pulsed laser deposition at 800 °C under 100 mTorr oxygen pressure. Before deposition, the substrates were etched in a NF_4F-buffered HF solution (NF_4F/HF = 7:1) for 45 s and annealed at 950 °C for 75 min in flowing O_2 to achieve a TiO_2-single-terminated (001) surface. The sheet carrier concentration is about $1.5 \times 10^{18}/cm^2$. A PLD 20 KrF excimer laser (Excimer, China), with a pulsed 248 nm output, was used to ablate a stoichiometric polycrystalline HZO target with a laser energy density of 1.5 J/cm^2 and a repetition rate of 2 Hz. The Pt top electrodes, 30 μm in diameter, were sputter-deposited using an AJA Orion-8-UHV sputtering system at room-temperature through a shadow mask. An Ohmic contact to the Nb:STO semiconductor electrode was made through a silver paste. Surface morphology of the HZO film was characterized using an Asylum Research Cypher ES atomic force microscope (AFM). The crystal structure of the junction was checked by grazing incident x-ray diffraction (GIXRD) using a Rigaku D/MAX-2500 diffractometer. The thickness of the HZO film was measured by x-ray reflection (XRR) using a Brucker D8 Discover diffractometer. Ferroelectric characteristics of the HZO films were measured by piezoresponse force microscopy (PFM) using the same AFM, and polarization–voltage (*P–V*) hysteresis loops were measured using a Radiant Precision Multiferroic system. The PFM amplitude and phase signals were acquired on the bared HZO film surface at room temperature using Pt coated cantilever probes (Nanoworld EFM), while the Nb:STO substrate was grounded. The resistance–voltage (*R–V*) loops were measured using a Keithley 2400 Sourcemeter.

Figure 1(b) shows a typical AFM image of the HZO film surface. The HZO film is smooth with the root mean square roughness acquired over a 3×3 μm^2 area less than 100 pm. The GIXRD measurement was performed with 2θ increasing from 20° to 50° to analyze the crystal structure of the HZO film. As shown in Fig. 1(c), the main diffraction features from the HZO film are two peaks at 28.6° and 30.09°, from the $(\bar{1}11)$ plane of a monoclinic (m-) phase and the (111) plane of an orthorhombic (o-) phase, respectively. Although the HZO film is polycrystalline with a mixed phase, the appearance of the o-phase indicates the formation of non-centrosymmetric ferroelectric HZO.[1] It is reported that HZO films grow epitaxially on $La_{0.67}Sr_{0.33}MnO_3$ (LSMO) buffered STO substrates.[4] Although the in-plane lattice parameter of Nb:STO is almost the same to that of LSMO deposed on the STO substrate, the HZO films here are polycrystalline. This indicates that lattice matching is not the key factor in determining the growth mode. It has been proposed that the chemical termination of LSMO has a great effect on the amount of an o-phase in the HZO film.[27] Figure 1(d) shows the XRR pattern of the HZO film. The clear Kiessig fringes indicate a smooth HZO surface and a sharp HZO/Nb:STO interface. By using GenX software to fit the Kiessig fringes,[28] the HZO film thickness can be extracted to be 5.8 nm.

Ferroelectric properties of the ultrathin barrier play a vital role in the performance of FTJs. Therefore, it is necessary to perform PFM and *P–V* hysteresis loop measurements to evaluate ferroelectric properties of the HZO barrier. Figures 2(a) and 2(b) show out-of-plane PFM phase and amplitude images over a 5×5 μm^2 area. Left and right half of the central 3×3 μm^2 area was poled by scanning the tip biased at +5 and −5 V, respectively, prior to the measurement. The

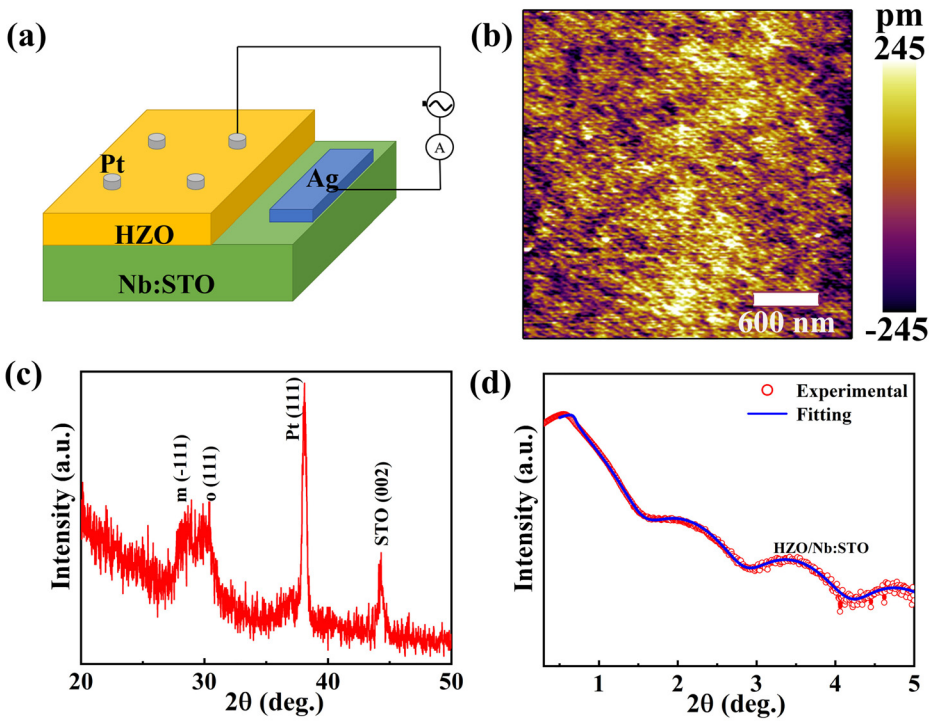

FIG. 1. (a) Schematic diagram of the Pt/HZO/Nb:STO FTJs, (b) surface morphology of the HZO film over a 3×3 μm^2 area, (c) GIXRD pattern of the Pt/HZO/Nb:STO FTJs, and (d) XRR pattern of the HZO film deposited on Nb:STO with fitting.

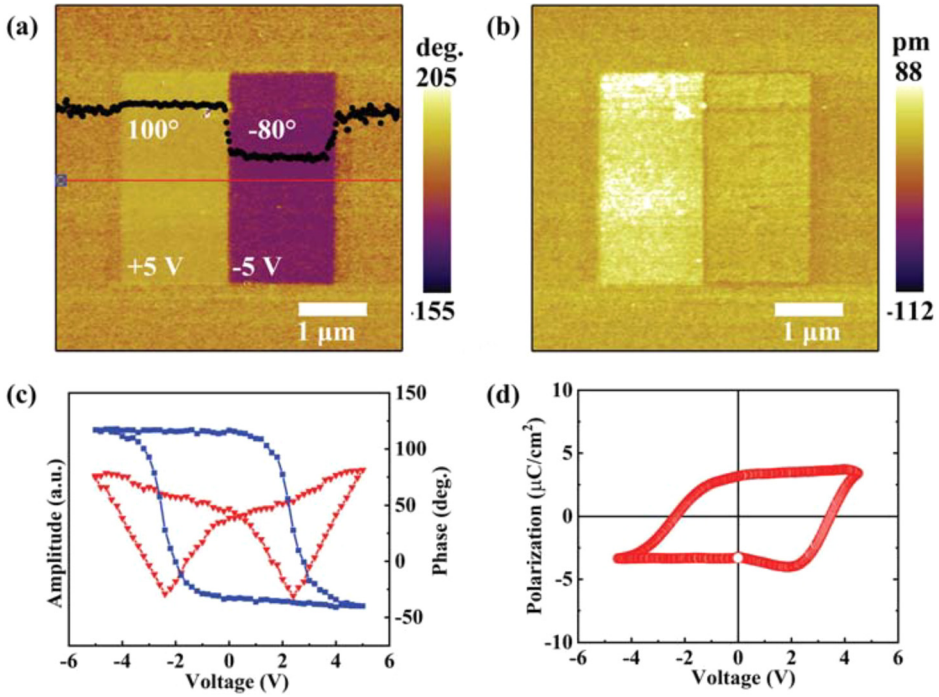

FIG. 2. Out-of-plane PFM phase (a) and amplitude (b) images of the HZO film, acquired after the left and right half of the central $3 \times 3\ \mu m^2$ area was scanned with the tip biased at +5 and −5 V, respectively. The inset shows the phase of the red line, (c) switching spectroscopy PFM phase (blue) and amplitude (red) loops of the HZO film, and (d) *P–V* hysteresis loop of the HZO film measured at 1 kHz.

180° phase shift in the phase image and clear domain boundaries in the amplitude image indicate that antiparallel domains can be written in the HZO film. The phase of the un-poled area is identical as that of the +5 V poled area, indicating that the as-deposited film is preferentially polarized downward. This is similar to $BiFeO_3$ films deposited on STO substrates, where the TiO_2-termination produces negative interface charges that induce the downward polarization.[29] Next, we performed switching spectroscopy PFM measurement on the film. The obtained phase and amplitude hysteresis loops are shown in Fig. 2(c). The coercive voltages of this 5.8 nm thick HZO film are ±2.4 V, determined from the two minima of the butterfly like amplitude loop. Figure 2(d) shows the *P–V* hysteresis loop of the HZO film without any wake-up pulses. This confirms the ferroelectricity of the HZO film. Under an applied voltage of 4.5 V, the remnant polarization is observed to be 3.5 $\mu C/cm^2$, in agreement with previous reports.[27] Compared with the remanent polarization around 34 $\mu C/cm^2$ in epitaxial HZO films deposed on LSMO/STO,[4] this film exhibits a rather small polarization. Since the polarization of HZO is along the c-axis of the o-phase, this may be the result of the low fraction of the ferroelectric o-phase in the film, consistent with the structure characterization.

Figure 3(a) shows a typical *R–V* curve of the Pt/HZO/Nb:STO FTJs. The device is written by pulses with 3 ms, and resistance is read by a pulse of 0.1 V and 5 ms after each write pulse. The junction is in the OFF state when no write pulse is applied. With increasing the write pulse amplitude, the junction resistance keeps constant at the initial state, until the pulse amplitude is greater than +2.7 V, at which the junction resistance falls to the ON state. With decreasing the write pulse amplitude, the device keeps at the ON state until it switches to the OFF state below −2.7 V. The electroresistance switching at ±2.7 V is in good agreement with the coercive voltage of the HZO film. This hysteretic *R–V* behavior indicates that the TER effect observed is associated with ferroelectric switching in the HZO barrier. The device is at ON (OFF) state when the polarization direction in the ferroelectric barrier is pointed toward (opposite to) the n-type semiconductor electrode, as revealed previously.[20] Our HZO-based FTJs show a TER ratio of 800, defined as R_{OFF}/R_{ON}. The current–voltage (*J–V*) curves collected after writing the FTJ device to the ON (OFF) state by a +3.5 (−3.5 V) pulse are shown in Fig. 3(b). In the ON state, the low-voltage part of the *J–V* curve can be well fitted to the direct tunneling current based on a trapezoidal potential barrier[30,31] using the equation

$$J \cong C\frac{\exp\left\{\alpha(V)\left[\left(\phi_2-\frac{eV}{2}\right)^{\frac{3}{2}}-\left(\phi_1+\frac{eV}{2}\right)^{\frac{3}{2}}\right]\right\}}{\alpha^2(V)\left[\left(\phi_2-\frac{eV}{2}\right)^{\frac{1}{2}}-\left(\phi_1+\frac{eV}{2}\right)^{\frac{1}{2}}\right]^2}\times\sinh\left\{\frac{3}{2}\alpha(V)\left[\left(\phi_2-\frac{eV}{2}\right)^{\frac{1}{2}}-\left(\phi_1+\frac{eV}{2}\right)^{\frac{1}{2}}\right]\frac{eV}{2}\right\}, \quad (1)$$

where $C=-\frac{4em^*m_e}{9\pi^2\hbar^3}$, $\alpha(V)\equiv\frac{[4d(2m^*m_e)^{\frac{1}{2}}]}{[3\hbar(\phi_1+eV-\phi_2)]}$, ϕ_1 (ϕ_2) is the barrier height at the Pt/HZO (HZO/Nb:STO) interface, $\hbar$ is the reduced Planck constant, d is the barrier width, e is the electron charge, m^* is the effective mass, and m_e is the electron mass. The fitted values are $\phi_1 = 2.25 \pm 0.07$ and $\phi_2 = 0.81 \pm 0.02$ eV, in good agreement with the experimental results previously reported.[21,32] This is reasonable because in the ON state, the semiconductor surface is accumulated with electrons and the tunneling electrons see only the barrier of HZO. In the OFF state, when the polarization of HZO film points opposite to the Nb:STO substrate, the *J–V* curve exhibits a thermally activated character and the junction transport characteristic can be fitted by[33]

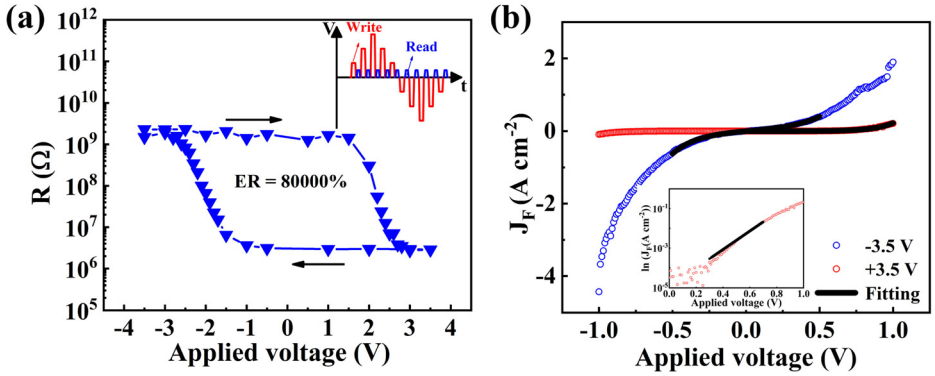

FIG. 3. (a) *R–V* hysteresis loop of the Pt/HZO/Nb:STO FTJs. The inset shows the pulse train for the measurement and (b) *J–V* curves measured at the ON and the OFF states with fittings. The inset is lnJ_F–*V* curve for the ON state and its fitting with Eq. (2).

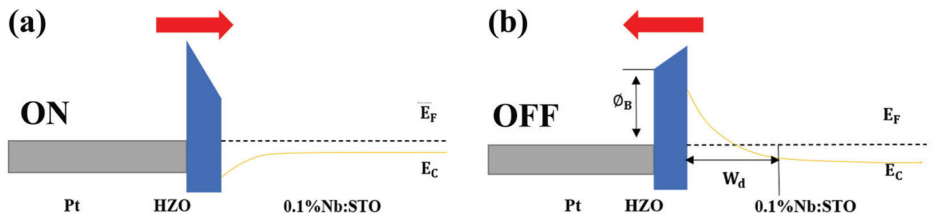

FIG. 4. Schematic illustrations of the electron band diagram of an MFS-type FTJ in (a) ON state and (b) OFF state according to the polarization direction.

$$J_F = J_0 \exp\left(\frac{eV}{nk_BT}\right), \quad (2)$$

where J_F is the forward current density, J_0 is the saturated current density, e is the electron charge, n is the ideality factor, k_B is the Boltzmann constant, and T is the absolute temperature. This indicates that at the OFF state, the Schottky barrier at the Nb:STO surface, due to the depletion of electrons, dominates the transport. The barrier profiles in the ON and the OFF states are shown schematically in Fig. 4.

To evaluate the reliability of the FTJs, resistance stability during long-time retention and data reproducibility over a large number of switching cycles are measured. Figure 5(a) displays the retention characteristic of the Pt/HZO/Nb:STO FTJs after +3.5 (−3.5 V) write pulse with 30 ms. There is no obvious degradation up to 10 000 s for both the ON and the OFF states. Figure 5(b) shows the ON and the OFF states' resistance as functions of switching cycles. Although the resistance of both states fluctuate, the TER ratio of the FTJ maintains approximately 100 after 1500 switching cycles by 3.5 V bipolar pulses with 3 ms. The reliability results indicate the potential of Pt/HZO/Nb:STO FTJs for nonvolatile memory applications.

In summary, polycrystalline HZO films, 5.8 nm in thickness, have been deposited on Nb:STO substrates and the nonvolatile memory effect of Pt/HZO/Nb:STO FTJ is characterized. PFM and hysteresis loops reveal robust ferroelectricity of these ultrathin HZO films. By using a Nb:STO semiconductor electrode, the TER ratio of the FTJs reaches 800 at ±3.5 V write pulses. Compared with the previously reported HfO_2-based metal/ferroelectric/semiconductor FTJs, the TER has been improved by an order of magnitude. By fitting the transport characteristics, it is observed that the ON state obeys direct tunneling, while the OFF state is dominated by thermal emission. The enhanced TER ratio is a result of the ferroelectric field effect that switches the Nb:STO semiconductor surface between accumulation and depletion. An additional Schottky barrier appears when the Nb:STO surface is depleted, resulting in a greater OFF state resistance. Meanwhile, the

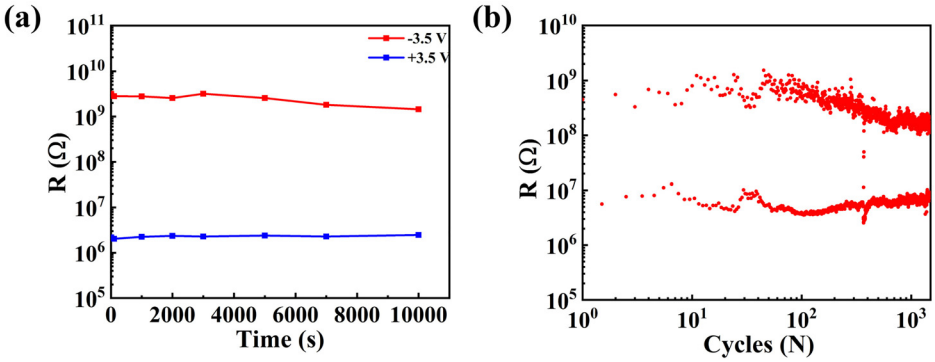

FIG. 5. (a) Retention characteristic of the Pt/HZO/Nb:STO FTJs and (b) ON and OFF resistances of the Pt/HZO/Nb:STO FTJs as functions of bipolar switching cycles.

Pt/HZO/Nb:STO FTJ exhibits long data retention up to 10 000 s and excellent endurance performance up to 1500 bipolar switches, making it a promising candidate for nonvolatile memories.

This work was sponsored by the Natural Science Foundation of China (Nos. 51725203, 51721001, and U1932115).

There are no conflicts to declare.

DATA AVAILABILITY

The data that support the findings of this study are available from the corresponding author upon reasonable request.

REFERENCES

[1]T. S. Böscke, J. Mller, D. Bräuhaus, U. Schröder, and U. Böttger, Appl. Phys. Lett. **99**, 102903 (2011).
[2]S. S. Cheema1, D. Kwon, N. Shanker, R. Reis, S.-L. Hsu, J. Xiao, H. Zhang, R. Wagner, A. Datar, M. R. McCarter, C. R. Serrao, A. K. Yadav, G. Karbasian, C.-H. Hsu, A. J. Tan, L.-C. Wang, V. Thakare, X. Zhang, A. Mehta, E. Karapetrova, R. V. Chopdekar, P. Shafer, E. Arenholz, C. Hu, R. Proksch, R. Ramesh, J. Ciston, and S. Salahuddin, Nature **580**, 478 (2020).
[3]J. Muller, P. Polakowski, S. Mueller, and T. Mikolajick, ECS J. Solid State Sci. Technol. **4**, N30 (2015).
[4]Y. Wei, P. Nukala, M. Salverda, S. Matzen, H. J. Zhao, J. Momand, A. Everhardt, G. R. Blake, P. Lecoeur, B. J. Kooi, J. Íñiguez, B. Dkhil, and B. Noheda, Nat. Mater. **17**, 1095 (2018).
[5]S. Mueller, J. Mueller, A. Singh, S. Riedel, J. Sundqvist, U. Schroeder, and T. Mikolajick, Adv. Funct. Mater. **22**, 2412 (2012).
[6]J. Muller, U. Schröoder, T. S. Böoscke, I. Möuller, U. Böottger, L. Wilde, J. Sundqvist, M. Lemberger, P. Kucher, T. Mikolajick, and L. Frey, J. Appl. Phys. **110**, 114113 (2011).
[7]X. Li, C. Li, Z. Xu, Y. Li, Y. Yang, H. Hu, Z. Jiang, J. Wang, J. Ren, C. Zheng, C. Lu, and Z. Wen, Phys. Status Solidi RRL **15**, 2000481 (2021).
[8]S. Mueller, C. Adelmann, A. Singh, S. V. Elshocht, U. Schroeder, and T. Mikolajick, ECS J. Solid St. Sci. **1**, 123 (2012).
[9]T. Schenk, S. Mueller, U. Schroeder, R. Materlik, A. Kersch, M. Popovici, C. Adelmann, S. Van Elshocht, and T. Mikolajick, in *Proceedings of the European Solid-State Device Research Conference, Bucharest, Romania, 16-20 September 2013* (IEEE, 2013), p. 260.
[10]Y. Zhang, Q. Yang, L. Tao, E. Y. Tsymbal, and V. Alexandrov, Phys. Rev. Appl. **14**, 014068 (2020).
[11]P. Polakowski, S. Riedel, W. Weinreich, M. Rudolf, J. Sundqvist, K. Seidel, and J. Müller, in IEEE 6th International Memory Workshop (2014), Vol. 1.
[12]K. Kim, Y. Kim, M. Park, H. Park, Y. Kwon, Y. Lee, H. Kim, T. Moon, Y. Lee, S. Hyun, B. Kim, and C. Hwang, Adv. Func. Mater. **29**, 1808228 (2019).
[13]C. Wu, H. Ye, B. Grisafe, S. Datta, and P. Fay, Phys. Status Solidi A **217**, 1900717 (2020).
[14]D. Das, V. Gaddam, and S. Jeon, IEEE Electron Device Lett. **42**, 331 (2021).
[15]Z. Wen and D. Wu, Adv. Mater. **32**, 1904123 (2020).
[16]V. Garcia and M. Bibes, Nat. Commun. **5**, 4289 (2014).
[17]L. Esaki, R. B. Laibowits, and P. J. Stiles, IBM Tech. Discl. Bull. **13**, 2161 (1971).
[18]Y. Yang, M. Wu, X. Li, H. Hu, Z. Jiang, Z. Li, X. Hao, C. Zheng, X. Lou, S. J. Pennycook, and Z. Wen, ACS Appl. Mater. Interfaces **12**, 32935 (2020).
[19]Z. Wen, C. Li, D. Wu, A. Li, and N. Ming, Nat. Mater. **12**, 617 (2013).
[20]Z. Xi, J. Ruan, C. Li, C. Zheng, Z. Wen, J. Dai, A. Li, and D. Wu, Nat. Commun. **8**, 15217 (2017).
[21]M. C. Sulzbach, S. Estandía, X. Long, J. Lyu, N. Dix, J. Gàzquez, M. F. Chisholm, F. Sánchez, I. Fina, and J. Fontcuberta, Adv. Electron. Mater. **6**, 1900852 (2020).
[22]M. C. Sulzbach, S. Estandía, J. Gàzquez, F. Sánchez, I. Fina, and J. Fontcuberta, Adv. Funct. Mater. **31**, 2002638 (2020).
[23]J. Li, N. Li, C. Ge, H. Huang, Y. Sun, P. Gao, M. He, C. Wang, G. Yang, and K. Jin, Science **16**, 368 (2019).
[24]C. Ma, Z. Luo, W. C. Huang, L. T. Zhao, Q. L. Chen, Y. Lin, X. Liu, Z. W. Chen, C. C. Liu, H. Y. Sun, X. Jin, Y. W. Yin, and X. G. Li, Nat. Commun. **11**, 1439 (2020).
[25]Y. Goh and S. Jeon, Nanotechnology **29**, 335201 (2018).
[26]J. Hwang, Y. Goh, and S. Jeon, IEEE Electron Device Lett. **41**, 1193 (2020).
[27]S. Estandía, J. Gàzquez, M. Varela, I. Fina, and F. Sánchez, J. Mater. Chem. C **9**, 3486 (2021).
[28]M. Bjöorck and G. Andersson, J. Appl. Crystallogr. **40**, 1174 (2007).
[29]P. Yu, W. Luo, D. Yi, J. X. Zhang, M. D. Rosselld, C.-H. Yang, L. Youg, S. J. Pennycookb, and R. Ramesh, Proc. Natl. Acad. U. S. A. **109**, 9710 (2012).
[30]W. F. Brinkman, R. C. Dynes, and J. M. Rowell, "Tunneling conductance of asymmetric barriers," J. Appl. Phys. **41**, 1915 (1970).
[31]A. Gruverman, D. Wu, H. Lu, Y. Wang, H. W. Jang, C. M. Folkman, M. Y. Zhuravlev, D. Felker, M. Rzchowski, C. B. Eom, and E. Y. Tsymbal, Nano Lett. **9**, 3539 (2009).
[32]F. Ambriz-Vargas, G. Kolhatkar, M. Broyer, A. Hadj-Youssef, R. Nouar, A. Sarkissian, R. Thomas, M. A. Gauthier, and A. Ruediger, ACS Appl. Mater. Interfaces **9**, 13262 (2017).
[33]L. Pintilie and M. Alexe, J. Appl. Phys. **98**, 124103 (2005).